

<sup>1</sup> **Cross-scale interaction of host tree size and climate governs bark  
2 beetle-induced tree mortality**

<sup>3</sup> Michael J. Koontz<sup>1,2,3\*</sup>, Andrew M. Latimer<sup>1,2</sup>, Leif A. Mortenson<sup>4</sup>, Christopher J. Fettig<sup>5</sup>, Malcolm P.  
<sup>4</sup> North<sup>1,2,6</sup>

<sup>5</sup> <sup>1</sup>Graduate Group in Ecology, University of California, Davis, CA, USA

<sup>6</sup> <sup>2</sup>Department of Plant Sciences, University of California, Davis, CA, USA

<sup>7</sup> <sup>3</sup>Earth Lab, University of Colorado-Boulder; Boulder, CO, USA

<sup>8</sup> <sup>4</sup>USDA Forest Service, Pacific Southwest Research Station, Placerville, CA, USA

<sup>9</sup> <sup>5</sup>USDA Forest Service, Pacific Southwest Research Station, Davis, CA, USA

<sup>10</sup> <sup>6</sup>USDA Forest Service, Pacific Southwest Research Station, Mammoth Lakes, CA, USA

<sup>11</sup> \*Correspondence: michael.koontz@colorado.edu

<sup>12</sup> *Keywords:* *Dendroctonus brevicomis*, disturbance, drones, *Pinus ponderosa*, Sierra Nevada, structure from motion, forest structure, climate change-type drought, macroecology

<sup>14</sup> *Abstract word count:* 310

<sup>15</sup> *Overall .docx word count:* 11499

<sup>16</sup> *Main text word count:* 4034 (Intro: 1264 Results: 368 (41+110+217); Discussion: 2402)

<sup>17</sup> *Methods word count:* 3093 (661+642+1463+327)

<sup>18</sup> *Text boxes word count:* 0

<sup>19</sup> Date report generated: April 30, 2020

<sup>20</sup> **Abstract**

<sup>21</sup> The Californian hot drought of 2012 to 2015 created favorable conditions for unprecedented ponderosa pine  
<sup>22</sup> (*Pinus ponderosa*) mortality in the Sierra Nevada mountain range, largely attributable to the western pine  
<sup>23</sup> beetle (*Dendroctonus brevicomis*; WPB). Climate conditions and forest density may interact to affect tree  
<sup>24</sup> mortality, but density is a coarse gauge of forest structure that can affect WPB behavior in a number of  
<sup>25</sup> ways. Measuring broad-scale climate conditions simultaneously with local forest composition and structure–  
<sup>26</sup> the spatial distribution and size of trees– will refine our understanding of how these variables interact, but  
<sup>27</sup> is generally expensive and/or labor-intensive. We use drone surveys over 32 distinct sites along a 350-km  
<sup>28</sup> latitudinal and 1000-m elevational gradient in western slope Sierra Nevada ponderosa pine/mixed-conifer

29 forests and structure from motion (SfM) photogrammetry to segment and classify more than 450,000 trees  
30 over 9 km<sup>2</sup> of forest with WPB-induced tree mortality. We validated the segmentation and classification with  
31 data from 160 coincident field plots (each 0.041 ha in area) throughout the 32 sites, with the caveat that  
32 dead trees were all classified as ponderosa pine. We modeled the probability of ponderosa pine mortality as a  
33 function of forest structure and composition and their interaction with site-level climatic water deficit (CWD),  
34 accounting for spatial covariance using exact Gaussian processes. A greater local proportion of host trees  
35 strongly increased the probability of host mortality, with greater host density amplifying this effect. Further,  
36 we found a strong interaction between host size and CWD such that larger trees increased the probability of  
37 host mortality at hot/dry sites, but smaller trees tended to drive mortality in cool/wet sites. Our results  
38 demonstrate a variable response of WPB to local forest structure and composition across an environmental  
39 gradient, which may help reconcile differences between observed ecosystem-wide tree mortality patterns and  
40 predictions from models based on coarser-scale forest structure. Climate change adaptation strategies should  
41 consider that future disturbance outcomes may depend on interactions between local forest structure and  
42 broad-scale environmental gradients, with the potential for cross-scale interactions that challenge our current  
43 understanding of forest insect dynamics.

## 44 Introduction

45 Bark beetles dealt the final blow to many of the nearly 150 million trees killed in the California hot drought of  
46 2012 to 2015 and its aftermath (USDAFS 2019). A harbinger of climate change effects to come, record high  
47 temperatures exacerbated the drought (Griffin and Anchukaitis 2014, Robeson 2015), which increased water  
48 stress in trees (???, Asner et al. 2016), making them more susceptible to colonization by bark beetles (Fettig  
49 2012, Kolb et al. 2016). Further, a century of fire suppression policy has enabled forests to grow unchecked,  
50 which can also make them more vulnerable to bark beetles (???, Fettig 2012, Restaino et al. 2019). This  
51 combination of environmental conditions and forest structural characteristics led to tree mortality events of  
52 unprecedented size across the state (???, Young et al. 2017). Tree mortality exhibited a strong latitudinal  
53 and elevational gradient (Asner et al. 2016, Young et al. 2017) that can only be partially explained by  
54 coarse-scale measures of environmental conditions (i.e., historic climatic water deficit; CWD) and current  
55 forest structure (i.e., current regional basal area) (Young et al. 2017). Progressive loss of canopy water  
56 content offers additional insight into tree vulnerability to mortality, but cannot ultimately resolve which  
57 trees die in forests with bark beetles as a key mortality agent (???). Bark beetles respond to local forest  
58 characteristics in positive feedbacks that non-linearly alter tree mortality dynamics against a background  
59 of environmental conditions that stress trees (Raffa et al. 2008, Boone et al. 2011). Thus, an explicit

60 consideration of local forest structure and composition (Stephenson et al. 2019, Fettig et al. 2019) as well as  
61 its cross-scale interaction with regional climate conditions (Senf et al. 2017) can refine our understanding of  
62 tree mortality patterns from California's recent hot drought. The challenge of simultaneously measuring the  
63 effects of both local-scale forest features (such as structure and composition) and broad-scale environmental  
64 conditions (such as climatic water deficit; CWD) on forest insect disturbance leaves their interaction effect  
65 relatively underexplored (Seidl et al. 2016, Senf et al. 2017, Stephenson et al. 2019, Fettig et al. 2019).

66 The ponderosa pine/mixed-conifer forests in California's Sierra Nevada region are characterized by regular  
67 bark beetle disturbances, primarily by the influence of western pine beetle (*Dendroctonus brevicomis*; WPB)  
68 on its host ponderosa pine (*Pinus ponderosa*) (Fettig 2016). WPB is a primary bark beetle— its reproductive  
69 success is contingent upon host tree mortality, which itself requires enough beetles to mass attack the host tree  
70 and overwhelm its defenses (Raffa and Berryman 1983). This Allee effect creates a strong coupling between  
71 beetle selection behavior of host trees and host tree susceptibility to colonization (Raffa and Berryman 1983,  
72 Logan et al. 1998, Wallin and Raffa 2004). A key defense mechanism of conifers to bark beetle attack is to  
73 flood beetle bore holes with resin, which physically expels colonizing beetles, can be toxic to the colonizers  
74 and their fungi, and may interrupt beetle communication (Franceschi et al. 2005, Raffa et al. 2015). Under  
75 normal conditions, weakened trees with compromised defenses are the most susceptible to colonization and  
76 will be the main targets of primary bark beetles like WPB (Bentz et al. 2010, Boone et al. 2011, Raffa  
77 et al. 2015). Under severe water stress, many trees no longer have the resources available to mount a  
78 defense (Boone et al. 2011, Kolb et al. 2016) and thus prolonged drought can often trigger increased bark  
79 beetle-induced tree mortality as average tree vigor declines (Bentz et al. 2010). As the local population  
80 density of beetles increases due to successful reproduction within spatially-aggregated weakened trees, as  
81 might occur during drought, mass attacks grow in size and become capable of overwhelming formidable tree  
82 defenses such that even healthy trees may be susceptible to colonization and mortality (Bentz et al. 2010,  
83 Boone et al. 2011, Raffa et al. 2015). Thus, water stress can be a key determinant of whether individual  
84 trees are susceptible to bark beetles under many conditions, and this environmental condition may interact  
85 with beetle population dynamics to drive tree susceptibility under extreme conditions (Bentz et al. 2010,  
86 Boone et al. 2011, Stephenson et al. 2019).

87 WPB activity is strongly influenced by forest structure— the spatial distribution and size of trees— and tree  
88 species composition. Taking forest structure alone, high-density forests are more prone to bark beetle-induced  
89 tree mortality (Fettig 2012) which may arise as greater competition for water resources amongst crowded trees  
90 and thus average tree resistance is lower (Hayes et al. 2009), or because smaller gaps between trees protect  
91 pheromone plumes from dissipation by the wind and thus enhance intraspecific beetle communication (Thistle

et al. 2004). Tree size is another aspect of forest structure that affects bark beetle host selection behavior with smaller trees tending to have lower capacity for resisting attack, and larger trees being more desirable targets on account of their thicker phloem providing greater nutritional content (Miller and Keen 1960, Chubaty et al. 2009, Boone et al. 2011, Graf et al. 2012). Throughout an outbreak, some bark beetle species will collectively “switch” the preferred size of tree to attack in order to navigate the trade-off between host susceptibility and host quality (Geiszler and Gara 1978, Klein et al. 1978, Mitchell and Preisler 1991, Preisler 1993, Wallin and Raffa 2004). Taking forest composition alone, WPB activity in the Sierra Nevada mountain range of California is necessarily tied to the regional distribution of its exclusive host, ponderosa pine (Fettig 2016). Colonization by primary bark beetles can also depend on the relative frequencies of tree species in a more local area, akin to reduced oligophagous insect herbivory in forests comprising taxonomically-distinct tree species compared to monocultures (Jactel and Brockerhoff 2007). The interaction between forest structure and composition also drives WPB activity. For instance, high-density forests with high host availability may experience greater beetle-induced tree mortality because dispersal distances between potential host trees are shorter reducing predation of adults searching for hosts and facilitating higher rates of colonization (Miller and Keen 1960, Berryman 1982, Fettig et al. 2007) or because high host availability reduces the chance of individual beetles wasting their limited resources flying to and landing on a non-host tree (Moeck et al. 1981, Evenden et al. 2014). Stand-scale measures of forest structure and composition thus paint a fundamentally limited picture of the mechanisms by which these forest characteristics affect bark beetle disturbance, but finer-grain information explicitly recognizing tree size, tree species, and local tree density should more appropriately capture the ecological processes underlying insect-induced tree mortality (Geiszler and Gara 1978, Mitchell and Preisler 1991, Preisler 1993, Kaiser et al. 2013). Additionally, considering the effects of local forest structure and composition with the effects of environmental conditions may help refine our understanding of tree mortality patterns in widespread events such as during the recent California hot drought.

The vast spatial extent of tree mortality in the 2012 to 2015 California hot drought challenges our ability to simultaneously consider how broad-scale environmental conditions may interact with local forest structure and composition to affect the dynamic between bark beetle selection and colonization of host trees, and host tree susceptibility to attack (Anderegg et al. 2015, Stephenson et al. 2019). Measuring local forest structure generally requires expensive instrumentation (Kane et al. 2014, Asner et al. 2016) or labor-intensive field surveys (Larson and Churchill 2012, Stephenson et al. 2019, Fettig et al. 2019), which constrains survey extent and frequency. Small, unhumanned aerial systems (sUAS) enable relatively fast and cheap remote imaging over hundreds of hectares of forest, which can be used to measure complex forest structure and

124 composition at the individual tree scale with Structure from Motion (SfM) photogrammetry (Morris et al.  
125 2017, Shiklomanov et al. 2019). The ultra-high resolution of sUAS-derived measurements as well as the  
126 ability to incorporate vegetation reflectance can help overcome challenges in species classification and dead  
127 tree detection inherent in other remote sensing methods, such as airborne LiDAR (Jeronimo et al. 2019).  
128 Distributing such surveys across an environmental gradient can overcome the data acquisition challenge  
129 inherent in investigating phenomena with both a strong local- and a strong broad-scale component.

130 We used sUAS-derived remote sensing images over a network of 32 sites in Sierra Nevada ponderosa pine/mixed-  
131 conifer forests spanning 1000 m of elevation and 350 km of latitude (see Fettig et al. 2019) and covering a  
132 total of 9 km<sup>2</sup> to ask how broad-scale environmental conditions interacted with local forest structure and  
133 composition to affect the probability of tree mortality during the cumulative tree mortality event of 2012 to  
134 2018. We asked:

- 135 1. How does the proportion of host trees in a local area and average host tree size affect WPB-induced  
136 tree mortality?
- 137 2. How does the density of all tree species (hereafter “overall density”) affect WPB-induced tree mortality?
- 138 3. How does environmentally-driven tree moisture stress affect WPB-induced tree mortality?
- 139 4. Do the effects of forest structure, forest composition, and environmental condition interact to influence  
140 WPB-induced tree mortality?

## 141 Methods

### 142 Study system

143 We built our study coincident with 160 vegetation/forest insect monitoring plots at 32 sites established  
144 between 2016 and 2017 by Fettig et al. (2019) (Figure 1). The study sites were chosen to reflect typical  
145 west-side Sierra Nevada yellow pine/mixed-conifer forests and were dominated by ponderosa pine (Fettig  
146 et al. 2019). Plots were located in WPB-attacked, yellow pine/mixed-conifer forests across the Eldorado,  
147 Stanislaus, Sierra and Sequoia National Forests and were stratified by elevation (914-1219 m, 1219-1524  
148 m, 1524-1829 m above sea level). In the Sequoia National Forest, the southernmost National Forest in our  
149 study, plots were stratified with the lowest elevation band of 1219-1524 m and extended to an upper elevation  
150 band of 1829-2134 m to capture a more similar forest community composition as at the more northern  
151 National Forests. The sites have variable forest structure and plot locations were selected in areas with >35%  
152 ponderosa pine basal area and >10% ponderosa pine mortality. At each site, five 0.041 ha circular plots

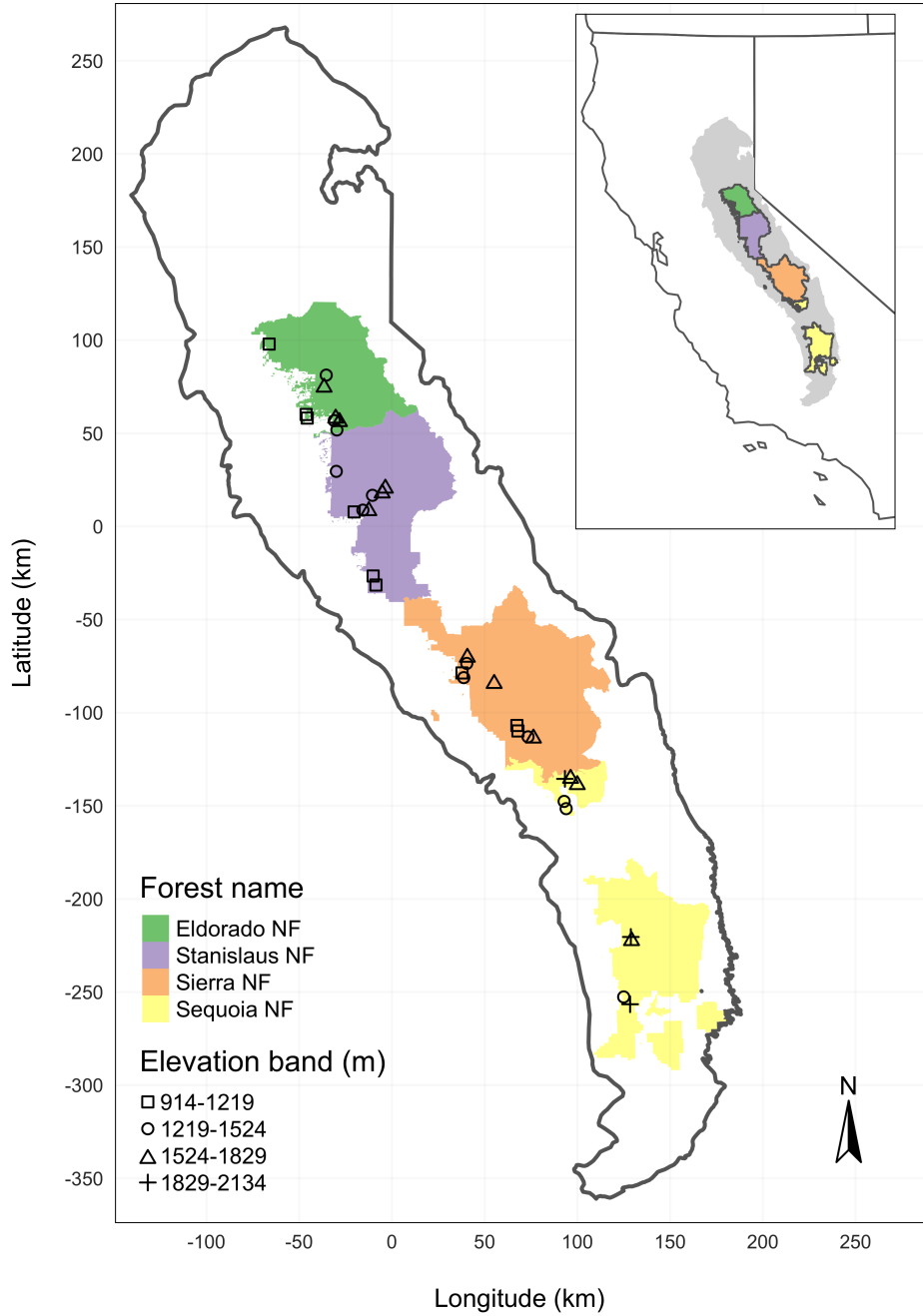


Figure 1: The network of field plots spanned a 350-km latitudinal gradient from the Eldorado National Forest in the north to the Sequoia National Forest in the south. Plots were stratified by three elevation bands in each forest, with the plots in the Sequoia National Forest (the southern-most National Forest) occupying elevation bands 305 m above the three bands in the other National Forests in order to capture a similar community composition.

were installed along transects with 80 to 200m between plots. In the field, Fettig et al. (2019) mapped all stem locations relative to the center of each plot using azimuth/distance measurements. Tree identity to species, tree height, and diameter at breast height (DBH) were recorded if DBH was greater than 6.35cm. Year of mortality was estimated based on needle color and retention if it occurred prior to plot establishment, and was directly observed thereafter during annual site visits. A small section of bark (approximately 625 cm<sup>2</sup>) on both north and south aspects was removed from dead trees to determine if bark beetle galleries were present. The shape, distribution, and orientation of galleries are commonly used to distinguish among bark beetle species (Fettig 2016). In some cases, deceased bark beetles were present beneath the bark to supplement identifications based on gallery formation. During the spring and early summer of 2018, all field plots were revisited to assess whether dead trees had fallen (Fettig et al. 2019).

In the typical life cycle of WPBs, females initiate host colonization by tunneling through the outer bark and into the phloem and outer xylem where they rupture resin canals.

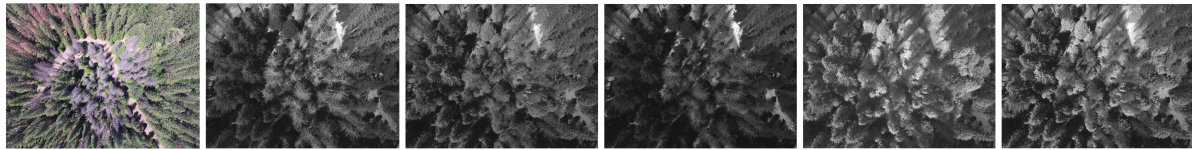
As a result, oleoresin exudes and collects on the bark surface, as is commonly observed with other bark beetle species. During the early stages of attack, females release an aggregation pheromone component which, in combination with host monoterpenes released from pitch tubes, is attractive to conspecifics (Bedard et al. 1969). An antiaggregation pheromone component is produced during latter stages of host colonization by several pathways, and is thought to reduce intraspecific competition by altering adult behavior to minimize overcrowding of developing brood within the host (Byers and Wood 1980). Volatiles from several nonhosts sympatric with ponderosa pine have been demonstrated to inhibit attraction of WPB to its aggregation pheromones (Shepherd et al. 2007, Fettig and Hilszczański 2015). In California, WPB generally has 2-3 generations in a single year and can often out-compete other primary bark beetles such as the mountain pine beetle (*Dendroctonus ponderosae*), in ponderosa pines, especially in larger trees (Miller and Keen 1960).

#### Aerial data collection and processing

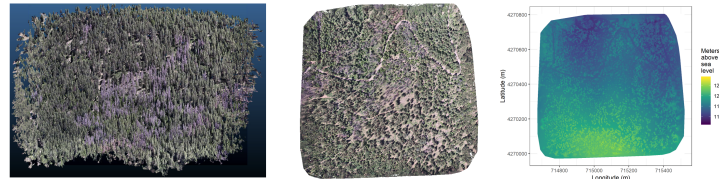
Nadir-facing imagery was captured using a gimbal-stabilized DJI Zenmuse X3 broad-band red/green/blue (RGB) camera (DJI 2015a) and a fixed-mounted Micasense Rededge3 multispectral camera with five narrow bands (Micasense 2015) on a DJI Matrice 100 aircraft (DJI 2015b). Imagery was captured from both cameras along preprogrammed aerial transects over ~40 hectares surrounding each of the 32 sites (each of these containing five field plots) and was processed in a series of steps to yield local forest structure and composition data suitable for our statistical analyses. All images were captured in 2018 during a 3-month period between early April and early July, and thus our work represents a postmortem investigation into the drivers of cumulative tree mortality through the course of the hot drought.

<sup>184</sup> Following the call by Wyngaard et al. (2019), we establish “data product levels” to reflect the image processing  
<sup>185</sup> pipeline from raw imagery (Level 0) to calibrated, fine-scale forest structure and composition information on  
<sup>186</sup> regular grids (Level 4), with each new data level derived from levels below it. Here, we outline the steps in the  
<sup>187</sup> processing and calibration pipeline visualized in Figure 2, and include additional details in the Supplemental  
<sup>188</sup> Information.

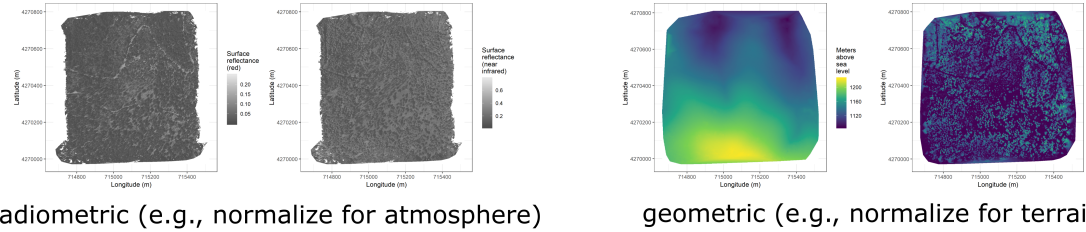
## Level 0: raw data from sensors



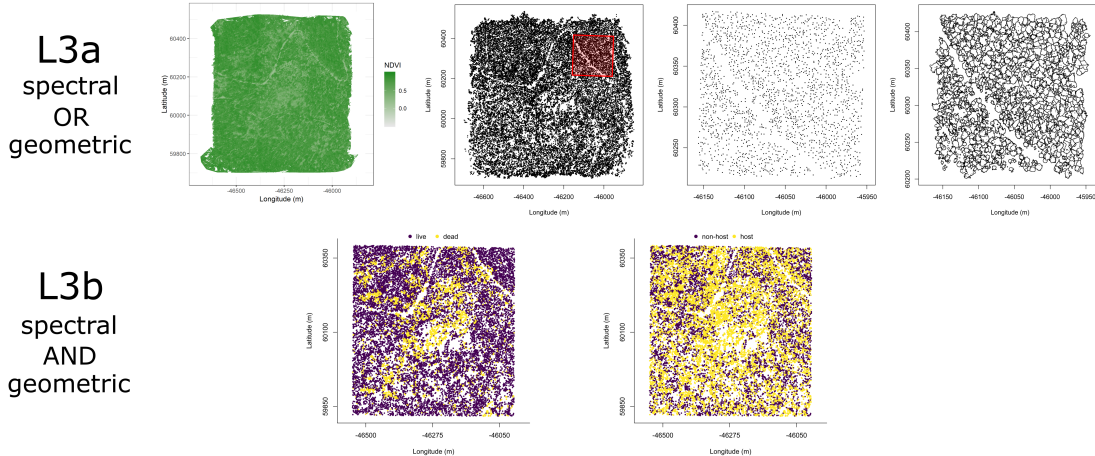
## Level 1: basic outputs from photogrammetric processing



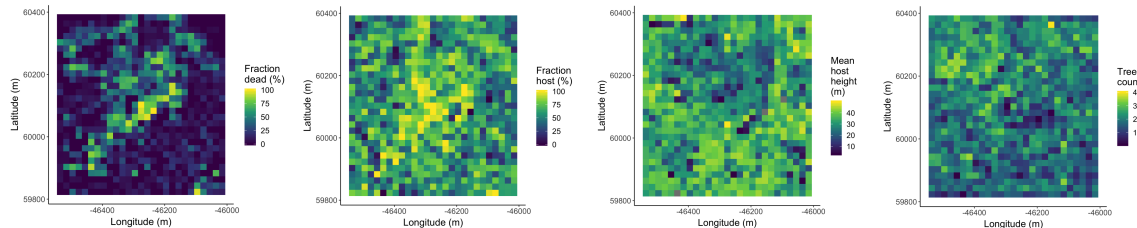
## Level 2: corrected outputs from photogrammetric processing



## Level 3: domain-specific information extraction



## Level 4: aggregations to regular grids



190 Figure 2. Schematic of the data processing workflow for a single site with each new data product level derived  
191 from data at lower levels.

192 Level 0 represents raw data from the sensors. From left to right: example broad-band RGB photo from  
193 DJI Zenmuse X3 camera, example blue photo from Rededge3 (centered on 475nm), example green photo  
194 from Rededge3 (centered on 560nm), example red photo from Rededge3 (centered on 668nm), example near  
195 infrared photo from Rededge3 (centered on 840nm), and example red edge photo from Rededge3 (centered on  
196 717nm).

197 Level 1 represents basic outputs from the photogrammetric workflow, in this case implemented with  
198 Pix4Dmapper. From left to right: a dense point cloud visualized in CloudCompare (<https://www.danielgm.net/cc/>), an orthophoto generated from the RGB camera, and a digital surface model representing the  
199 altitude above sea level (ground height + vegetation height) for every cell.  
200

201 Level 2 represents outputs from photogrammetric processing that have been corrected radiometrically or  
202 geometrically. From left to right: a radiometrically-corrected surface reflectance map of the red narrow band  
203 from the Rededge3 camera, a radiometrically-corrected surface reflectance map of the near infrared narrow  
204 band from the Rededge3 camera, a rasterized version of the digital terrain model derived by a geometric  
205 correction of the dense point cloud, and a canopy height model derived by subtracting the terrain height  
206 from the digital surface model.

207 Level 3 represents domain-specific information extraction from Level 2 products and is divided into two  
208 sub-levels. Level 3a products are derived using only spectral or only geometric data. From left to right: a  
209 reflectance map of Normalized Difference Vegetation Index (NDVI; Rouse et al. (1973)) derived using the red  
210 and near infrared Level 2 reflectance products, a map of points representing detected trees from the canopy  
211 height model with a red polygon highlighting the area presented in more detail for the next two images, a  
212 close-up of points representing detected trees, and a close-up of polygons representing segmented tree crowns.  
213 Level 3b products are derived using both spectral and geometric data. From left to right: a map of the point  
214 locations of detected trees that have been classified as alive or dead based on the pixel values within each  
215 segmented tree crown and a map of the point locations of detected trees classified to WPB host/non-host  
216 using the same spectral information. Note that our study relies on the generation of Level 3a products in  
217 order to combine them and create Level 3b products, but this need not be the case. For instance, deep  
218 learning/neural net methods may be able to use both the spectral and geometric information from Level 2  
219 simultaneously to locate and classify trees in a scene and directly generate Level 3b products without a need  
220 to first generate the Level 3a products shown in this schematic (Weinstein et al. 2019, dos Santos et al. 2019).

221 Level 4 represents aggregations of Level 3 products to regular grids which might better reflect the grain size  
222 of the data for which we have the best calibration and thus the most confidence or which might provide  
223 new information not possible at an individual-tree level (e.g., average distance between trees in a small  
224 neighborhood). From left to right: aggregation of live/dead classified trees as fraction of dead trees in a 20 x  
225 20-m cell, aggregation of host/non-host classified trees as fraction of hosts in a 20 x 20-m cell, aggregation of  
226 mean host height in a 20 x 20-m cell, and aggregation of tree count (including all species), in a 20 x 20-m  
227 cell. In our case, the 20 x 20-m aggregation produces a grid cell with an area of 400 m<sup>2</sup>, which most closely  
228 matches the 404-m<sup>2</sup> area of the ground-based vegetation plots whose data we used in an aggregated form to  
229 calibrate our derivation of Level 3 products.

#### 230 **Level 0: Raw data from sensors**

231 Raw data comprised approximately 1900 images per camera lens (one broad-band RGB lens and five narrow-  
232 band multispectral lenses) for each of the 32 sites (Figure 2; Level 0). Prior to the aerial survey, two strips of  
233 bright orange drop cloth (~100 x 15 cm) were positioned as an “X” over the permanent monuments marking  
234 the center of the 5 field plots from Fettig et al. (2019) (see Supplemental Information).

235 We preprogrammed north-south aerial transects using Map Pilot for DJI on iOS flight software (Drones-  
236 MadeEasy 2018) at an altitude of 120 m above ground level (with “ground” defined using a 1-arc-second  
237 digital elevation model (Farr et al. 2007)). The resulting ground sampling distance was approximately 5  
238 cm/px for the Zenmuse X3 RGB camera and approximately 8 cm/px for the Rededge3 multispectral camera.  
239 We used 91.6% image overlap (both forward and side) at the ground for the Zenmuse X3 RGB camera and  
240 83.9% overlap (forward and side) for the Rededge3 multispectral camera.

#### 241 **Level 1: Basic outputs from photogrammetric processing**

242 We used SfM photogrammetry implemented in Pix4Dmapper Cloud ([www.pix4d.com](http://www.pix4d.com)) to generate dense point  
243 clouds (Figure 2; Level 1, left), orthophotos (Figure 2; Level 1, center), and digital surface models (Figure 2;  
244 Level 1, right) for each field site (Frey et al. 2018). For 29 sites, we processed the Rededge3 multispectral  
245 imagery alone to generate these products. For three sites, we processed the RGB and the multispectral  
246 imagery together to enhance the point density of the dense point cloud. All SfM projects resulted in a single  
247 processing “block,” indicating that all images in the project were optimized and processed together. The  
248 dense point cloud represents x, y, and z coordinates as well as the color of millions of points per site. The  
249 orthophoto represents a radiometrically uncalibrated, top-down view of the survey site that preserves the

250 relative x-y positions of objects in the scene. The digital surface model is a rasterized version of the dense  
251 point cloud that shows the altitude above sea level for each pixel in the scene at the ground sampling distance  
252 of the camera that generated the Level 0 data.

253 **Level 2: Corrected outputs from photogrammetric processing**

254 **Radiometric corrections**

255 A radiometrically-corrected reflectance map (Figure 2; Level 2, left two figures; i.e., a corrected version of the  
256 Level 1 orthophoto) was generated using the Pix4D software by incorporating incoming light conditions for  
257 each narrow band of the Rededge3 camera (captured simultaneously with the Rededge3 camera using an  
258 integrated downwelling light sensor) as well as a pre-flight image of a calibration panel of known reflectance  
259 (see Supplemental Information for camera and calibration panel details).

260 **Geometric corrections**

261 We implemented a geometric correction to the Level 1 dense point cloud and digital surface model by  
262 normalizing these data for the terrain underneath the vegetation. We generated the digital terrain model  
263 representing the ground underneath the vegetation at 1-m resolution (Figure 2; Level 2, third image) by  
264 classifying each survey area's dense point cloud into "ground" and "non-ground" points using a cloth simulation  
265 filter algorithm (Zhang et al. 2016) implemented in the `lidR` (Roussel et al. 2019) package and rasterizing  
266 the ground points using the `raster` package (Hijmans et al. 2019). We generated a canopy height model  
267 (Figure 2; Level 2, fourth image) by subtracting the digital terrain model from the digital surface model.

268 **Level 3: Domain-specific information extraction**

269 **Level 3a: Data derived from spectral OR geometric Level 2 product**

270 Using just the spectral information from the radiometrically-corrected reflectance maps, we calculated several  
271 vegetation indices including the normalized difference vegetation index (NDVI; Rouse et al. (1973); Figure  
272 2; Level 3a, first image), the normalized difference red edge (NDRE; Gitelson and Merzlyak (1994)), the  
273 red-green index (RGI; Coops et al. (2006)), the red edge chlorophyll index ( $CI_{red\ edge}$ ; Clevers and Gitelson  
274 (2013)), and the green chlorophyll index ( $CI_{green}$ ; Clevers and Gitelson (2013)).

Table 1: Algorithm name, number of parameter sets tested for each algorithm, and references.

Algorithm	Parameter sets tested	Reference(s)
li2012	131	Li et al. (2012); Jakubowski et al. (2013); Shin et al. (2018)
lmfx	30	Roussel (2019)
localMaxima	6	Roussel et al. (2019)
multichm	1	Eysn et al. (2015)
ptrees	3	Vega et al. (2014)
vwf	3	Plowright (2018)
watershed	3	Pau et al. (2010)

275 Using just the geometric information from the canopy height model or terrain-normalized dense point cloud,  
 276 we generated maps of detected trees (Figure 2; Level 3a, second and third images) by testing a total of 7  
 277 automatic tree detection algorithms and a total of 177 parameter sets (Table 1). We used the field plot data  
 278 to assess each tree detection algorithm/parameter set by converting the distance-from-center and azimuth  
 279 measurements of the trees in the field plots to x-y positions relative to the field plot centers distinguishable in  
 280 the Level 2 reflectance maps as the orange fabric X’s that we laid out prior to each flight. In the reflectance  
 281 maps, we located 220 out of 160 field plot centers while some plot centers were obscured due to dense  
 282 interlocking tree crowns or because a plot center was located directly under a single tree crown. For each of  
 283 the 220 field plots with identifiable plot centers— the “validation field plots”, we calculated 7 forest structure  
 284 metrics using the ground data collected by Fettig et al. (2019): total number of trees, number of trees greater  
 285 than 15 m in height, mean height of trees, 25<sup>th</sup> percentile tree height, 75<sup>th</sup> percentile tree height, mean  
 286 distance to nearest tree neighbor, and mean distance to second nearest neighbor. For each tree detection  
 287 algorithm and parameter set described above, we calculated the same set of 7 structure metrics within the  
 288 footprint of the validation field plots. We calculated the Pearson’s correlation and root mean square error  
 289 (RMSE) between the ground data and the aerial data for each of the 7 structure metrics for each of the 177  
 290 automatic tree detection algorithms/parameter sets. For each algorithm and parameter set, we calculated its  
 291 performance relative to other algorithms as whether its Pearson’s correlation was within 5% of the highest  
 292 Pearson’s correlation as well as whether its RMSE was within 5% of the lowest RMSE. We summed the  
 293 number of forest structure metrics for which it reached these 5% thresholds for each algorithm/parameter  
 294 set. For automatically detecting trees across the whole study, we selected the algorithm/parameter set that

295 performed well across the most number of forest metrics (see Results).

296 We delineated individual tree crowns (Figure 2; Level 3a, fourth image) with a marker controlled watershed  
297 segmentation algorithm (Meyer and Beucher 1990) implemented in the **ForestTools** package (Plowright  
298 2018) using the detected treetops as markers. If the automatic segmentation algorithm failed to generate  
299 a crown segment for a detected tree (e.g., often snags with a very small crown footprint), a circular crown  
300 was generated with a radius of 0.5 m. If the segmentation generated multiple polygons for a single detected  
301 tree, only the polygon containing the detected tree was retained. Because image overlap decreases near the  
302 edges of the overall flight path and reduces the quality of the SfM processing in those areas, we excluded  
303 segmented crowns within 35 m of the edge of the survey area. Given the narrower field of view of the  
304 Rededge3 multispectral camera versus the X3 RGB camera whose optical parameters were used to define the  
305 ~40 hectare survey area around each site, as well as the 35 m additional buffering, the survey area at each  
306 site was ~30 ha (see Supplemental Information).

### 307 **Level 3b: Data derived from spectral AND geometric information**

308 We overlaid the segmented crowns on the reflectance maps from 20 sites spanning the latitudinal and elevation  
309 gradient in the study. Using QGIS (<https://qgis.org/en/site/>), we hand classified 564 trees as live/dead  
310 (Figure 3) and as one of 5 dominant species in the study area (ponderosa pine, *Pinus lambertiana*, *Abies*  
311 *concolor*, *Calocedrus decurrens*, or *Quercus kelloggii*) using the mapped ground data as a guide. Each tree was  
312 further classified as “host” for ponderosa pine or “non-host” for all other species (Fettig 2016). We extracted  
313 all the pixel values within each segmented crown polygon from the five, Level 2 orthorectified reflectance  
314 maps (one per narrow band on the Rededge3 camera) as well as from the five, Level 3a vegetation index  
315 maps using the **velox** package (Hunziker 2017). For each crown polygon, we calculated the mean value of the  
316 extracted Level 2 and Level 3a pixels and used them as ten independent variables in a five-fold cross validated  
317 boosted logistic regression model to predict whether the hand classified trees were alive or dead. For just the  
318 living trees, we similarly used all 10 mean reflectance values per crown polygon to predict tree species using a  
319 five-fold cross validated regularized discriminant analysis. The boosted logistic regression and regularized  
320 discriminant analysis were implemented using the **caret** package in R (Kuhn 2008). We used these models to  
321 classify all tree crowns in the data set as alive or dead (Figure 2; Level 3b, first image) as well as the species  
322 of living trees (Figure 2; Level 3b, second image). Finally, we estimated the basal area of each tree from their  
323 photogrammetry-derived height using species-specific simple linear regressions of the relationship between  
324 height and diameter at breast height as measured in the coincident field plots from Fettig et al. (2019).

325 **Level 4: Aggregations to regular grids**

326 We rasterized the forest structure and composition data at a spatial resolution similar to that of the field  
327 plots to better match the grain size at which we validated the automatic tree detection algorithms. In each  
328 raster cell, we calculated: number of dead trees, number of ponderosa pine trees, total number of trees, and  
329 mean height of ponderosa pine trees. The values of these variables in each grid cell and derivatives from  
330 them were used for visualization and modeling. Here, we show the fraction of dead trees per cell (Figure 2;  
331 Level 4, first image), the fraction of host trees per cell (Figure 2; Level 4, second image), the mean height of  
332 ponderosa pine trees in each cell (Figure 2; Level 4, third image), and the total count of trees per cell (Figure  
333 2; Level 4, fourth image).

334 **Note on assumptions about dead trees**

335 For the purposes of this study, we assumed that all dead trees were ponderosa pine and thus hosts colonized  
336 by WPB. This is a reasonably good assumption for our study area; for example, Fettig et al. (2019) found  
337 that 73.4% of dead trees in their coincident field plots were ponderosa pine. Mortality was concentrated in  
338 the larger-diameter classes and attributed primarily to WPB (see Figure 5 of Fettig et al. 2019). The species  
339 contributing to the next highest proportion of dead trees was incense cedar which represented 18.72% of the  
340 dead trees in the field plots. While the detected mortality is most likely to be ponderosa pine killed by WPB,  
341 it is critical to interpret our results with these limitations in mind.

342 **Environmental data**

343 We used CWD (Stephenson 1998) from the 1981-2010 mean value of the basin characterization model (Flint  
344 et al. 2013) as an integrated measure of temperature and moisture conditions for each of the 32 sites. Higher  
345 values of CWD correspond to hotter, drier conditions and lower values correspond to cooler, wetter conditions.  
346 CWD has been shown to correlate well with broad patterns of tree mortality in the Sierra Nevada (Young et  
347 al. 2017) as well as bark beetle-induced tree mortality (Millar et al. 2012). The forests along the entire CWD  
348 gradient used in this study experienced exceptional hot drought between 2012 to 2015 with a severity of at  
349 least a 1,200-year event, and perhaps more severe than a 10,000-year event (Griffin and Anchukaitis 2014,  
350 Robeson 2015). We converted the CWD value for each site into a z-score representing that site's deviation  
351 from the mean CWD across the climatic range of Sierra Nevada ponderosa pine as determined from 179  
352 herbarium records described in Baldwin et al. (2017). Thus, a CWD z-score of 1 would indicate that the

353 CWD at that site is one standard deviation hotter/drier than the mean CWD across all geolocated herbarium  
 354 records for ponderosa pine in the Sierra Nevada.

355 **Statistical model**

356 We used a generalized linear model with a zero-inflated binomial response and a logit link to predict the  
 357 probability of ponderosa pine mortality within each 20 x 20-m cell using the total number of ponderosa  
 358 pine trees in each cell as the number of trials, and the number of dead trees in each cell as the number of  
 359 “successes”. As covariates, we used the proportion of trees that are WPB hosts (i.e., ponderosa pine) in each  
 360 cell, the mean height of ponderosa pine trees in each cell, the count of trees of all species (overall density) in  
 361 each cell, and the site-level CWD using Eq. 1. Note that the two-way interaction between the overall density  
 362 and the proportion of trees that are hosts is directly proportional to the number of ponderosa pine trees in  
 363 the cell. We centered and scaled all predictor values, and used weakly-regularizing default priors from the  
 364 `brms` package (Bürkner 2017). To measure and account for spatial autocorrelation underlying ponderosa pine  
 365 mortality, we subsampled the data at each site to a random selection of 200, 20 x 20-m cells representing  
 366 approximately 27.5% of the surveyed area. Additionally with these subsampled data, we included a separate  
 367 exact Gaussian process term per site of the noncentered/nonscaled interaction between the x- and y-position  
 368 of each cell using the `gp()` function in the `brms` package (Bürkner 2017). The Gaussian process estimates the  
 369 spatial covariance in the response variable (log-odds of ponderosa pine mortality) jointly with the effects of  
 370 the other covariates.

$$y_{i,j} \sim \begin{cases} 0, & p \\ Binom(n_i, \pi_i), & 1 - p \end{cases}$$

$$\begin{aligned} logit(\pi_i) = & \beta_0 + \\ & \beta_1 X_{cwd,j} + \beta_2 X_{propHost,i} + \beta_3 X_{PipoHeight,i} + \\ & \beta_4 X_{overallDensity,i} + \beta_5 X_{overallBA,i} + \\ & \beta_6 X_{cwd,j} X_{PipoHeight,i} + \beta_7 X_{cwd,j} X_{propHost,i} + \\ & \beta_8 X_{cwd,j} X_{overallDensity,i} + \beta_9 X_{cwd,j} X_{overallBA,i} + \\ & \beta_{10} X_{propHost,i} X_{PipoHeight,i} + \beta_{11} X_{propHost,i} X_{overallDensity,i} + \\ & \beta_{12} X_{cwd,j} X_{propHost,i} X_{PipoHeight,i} + \\ & \mathcal{GP}_j(x_i, y_i) \end{aligned}$$

371 Where  $y_i$  is the number of dead trees in cell  $i$ ,  $n_i$  is the sum of the dead trees (assumed to be ponderosa pine)  
372 and live ponderosa pine trees in cell  $i$ ,  $\pi_i$  is the probability of ponderosa pine tree mortality in cell  $i$ ,  $p$  is the  
373 probability of there being zero dead trees in a cell arising as a result of an independent, unmodeled process,  
374  $X_{cwd,j}$  is the z-score of CWD for site  $j$ ,  $X_{propHost,i}$  is the scaled proportion of trees that are ponderosa pine  
375 in cell  $i$ ,  $X_{PipoHeight,i}$  is the scaled mean height of ponderosa pine trees in cell  $i$ ,  $X_{overallDensity,i}$  is the scaled  
376 density of all trees in cell  $i$ ,  $X_{overallBA,i}$  is the scaled basal area of all trees in cell  $i$ ,  $x_i$  and  $y_i$  are the x- and  
377 y- coordinates of the centroid of the cell in an EPSG3310 coordinate reference system, and  $\mathcal{GP}_j$  represents  
378 the exact Gaussian process describing the spatial covariance between cells at site  $j$ .

379 We fit this model using the **brms** package (Bürkner 2017) which implements the No U-Turn Sampler extension  
380 to the Hamiltonian Monte Carlo algorithm (Hoffman and Gelman 2014) in the Stan programming language  
381 (Carpenter et al. 2017). We used 4 chains with 4000 iterations each (2000 warmup, 2000 samples), and  
382 confirmed chain convergence by ensuring all `Rhat` values were less than 1.1 (Brooks and Gelman 1998) and  
383 that the bulk and tail effective sample sizes (ESS) for each estimated parameter were greater than 100 times  
384 the number of chains (i.e., greater than 400 in our case). We used posterior predictive checks to visually  
385 confirm model performance by overlaying the density curves of the predicted number of dead trees per cell  
386 over the observed number (Gabry et al. 2019). For the posterior predictive checks, we used 50 random  
387 samples from the model fit to generate 50 density curves and ensured curves were centered on the observed  
388 distribution, paying special attention to model performance at capturing counts of zero.

### 389 Software and data availability

390 All data are available via the Open Science Framework. Statistical analyses were performed using the **brms**  
391 packages. With the exception of the SfM software (Pix4Dmapper Cloud) and the GIS software QGIS, all  
392 data carpentry and analyses were performed using R (R Core Team 2018).

## 393 Results

### 394 Tree detection algorithm performance

395 We found that the experimental `lmfx` algorithm with parameter values of `dist2d = 1` and `ws = 2.5` (Roussel  
396 et al. 2019) performed the best across 7 measures of forest structure as measured by Pearson's correlation  
397 with ground data (Table 2).

Table 2: Correlation and differences between the best performing tree detection algorithm (lmfx with dist2d = 1 and ws = 2.5) and the ground data. An asterisk next to the correlation or RMSE indicates that this value was within 5% of the value of the best-performing algorithm/parameter set. Ground mean represents the mean value of the forest metric across the 220 field plots that were visible from the sUAS-derived imagery. The median error is calculated as the median of the differences between the air and ground values for the 220 visible plots. Thus, a positive number indicates an overestimate by the sUAS workflow and a negative number indicates an underestimate.

Forest structure metric	Ground mean	Correlation with ground	RMSE	Median error
total tree count	19	0.67*	8.68*	2
count of trees > 15 m	9.9	0.43	7.38	0
distance to 1st neighbor (m)	2.8	0.55*	1.16*	0.26
distance to 2nd neighbor (m)	4.3	0.61*	1.70*	0.12
height (m); 25 <sup>th</sup> percentile	12	0.16	8.46	-1.2
height (m); mean	18	0.29	7.81*	-2.3
height (m); 75 <sup>th</sup> percentile	25	0.35	10.33*	-4

### **398 Classification accuracy for live/dead and host/non-host**

399 The accuracy of live/dead classification on a withheld test dataset was 96.4%. The accuracy of species  
 400 classification on a withheld testing dataset was 64.1%. The accuracy of WPB host/non-WPB-host (i.e.,  
 401 ponderosa pine versus other tree species) on a withheld testing dataset was 71.8%.

### **402 Site summary based on best tree detection algorithm and classification**

403 Across all study sites, we detected, segmented, and classified 452,413 trees. Of these trees, we classified  
 404 118,879 as dead (26.3% mortality). Estimated site-level tree mortality ranged from 6.8% to 53.6%. See  
 405 Supplemental Information for site summaries and comparisons to site-level mortality measured from field  
 406 data.

### **407 Effect of local structure and regional climate on tree mortality attributed to western pine 408 beetle**

409 We detected a positive main effect of CWD on the probability of ponderosa pine mortality within each 20 x  
 410 20-m cell (Figure 4). We found a positive main effect of proportion of host trees per cell (effect size: 0.76;  
 411 95% CI: [0.70, 0.82]), with a greater proportion of host trees (i.e., ponderosa pine) in a cell increasing the

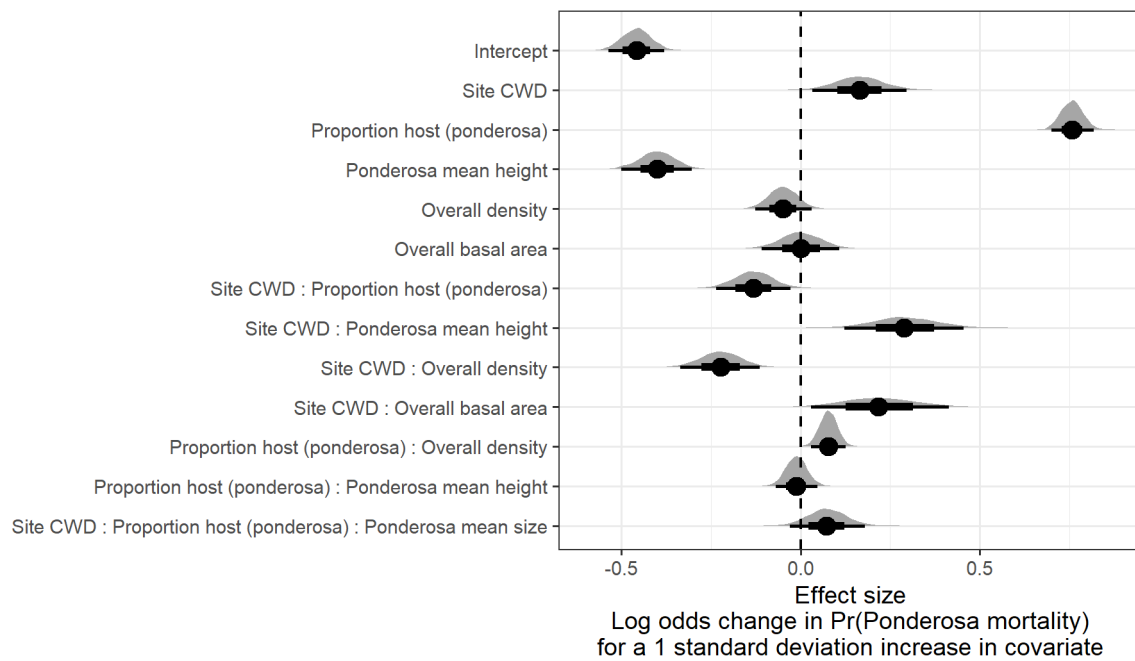


Figure 4: Posterior distributions of effect size from zero-inflated binomial model predicting the probability of ponderosa pine mortality in a 20 x 20-m cell given forest structure characteristics and site-level climatic water deficit (CWD). The gray filled area for each model covariate represents the probability density of the posterior distribution, the point underneath each density curve represents the median of the estimate, the bold interval surrounding the point estimate represents the 66% credible interval, and the thin interval surrounding the point estimate represents the 95% credible interval.

412 probability of ponderosa pine mortality. We detected no effect of overall tree density nor overall basal area  
413 (i.e., including both ponderosa pine and non-host species; tree density effect size: -0.05; 95% CI: [-0.13, 0.03];  
414 basal area effect size: 0.00; 95% CI: [-0.11, 0.11]).

415 We found a positive two-way interaction between the overall tree density per cell and the proportion of trees  
416 that were hosts, which is equivalent to a positive effect of the density of host trees (effect size: 0.08; 95% CI:  
417 [0.03, 0.13]; Figure 4).

418 We found a negative effect of mean height of ponderosa pine on the probability of ponderosa mortality,  
419 suggesting that WPB attacked smaller trees, on average (effect size: -0.40; 95% CI: [-0.50, -0.30]). However,  
420 there was a positive interaction between CWD and ponderosa pine mean height, such that larger trees were  
421 more likely to increase the local probability of ponderosa mortality in hotter, drier sites (effect size: 0.29;  
422 95% CI: [0.12, 0.46]; Figure 5).

423 We found weakly negative effects of the site-level CWD interactions with both the proportion of host trees  
424 and overall tree density (CWD/proportion host interaction effect size: -0.13; 95% CI: [-0.23, -0.03]; Figure 4;  
425 CWD/overall tree density interaction effect size: -0.22; 95% CI: [-0.34, -0.11]; Figure 4; Figure 5). We found  
426 a positive effect of the interaction between CWD and total basal area (effect size: 0.22; 95% CI: [0.03, 0.42];  
427 Figure 4; Figure 5).

## 428 Discussion

429 This study represents a novel use of drones to further our understanding of the simultaneous effects of  
430 local forest structure and composition with broad-scale environmental gradients on tree mortality attributed  
431 to WPB. We found strong positive effects (effect sizes >0.4) of both the proportion of host trees and the  
432 interaction between site CWD and host tree mean size (height) on the probability of ponderosa pine mortality.  
433 Conversely, we found a strong negative effect (effect size <-0.4) of mean height of ponderosa pine. Site-level  
434 CWD exerted a positive, but relatively weak, main effect on the probability of ponderosa mortality (effect  
435 size: 0.16; 95% CI: [0.03, 0.30]). To that end, we did not measure tree water stress at an individual tree  
436 level as in other recent work (Stephenson et al. 2019), and instead treated CWD as a general indicator of  
437 tree stress following results of coarser-scale studies (e.g., Young et al. 2017), which may have contributed to  
438 our failure to detect a stronger CWD effect. Also, our entire study area experienced the same extreme hot  
439 drought between 2012 and 2015 and the variation of mortality explained by a main effect of CWD may be  
440 dampened when most trees are experiencing a high degree of water stress (Floyd et al. 2009, Fettig et al.  
441 2019).

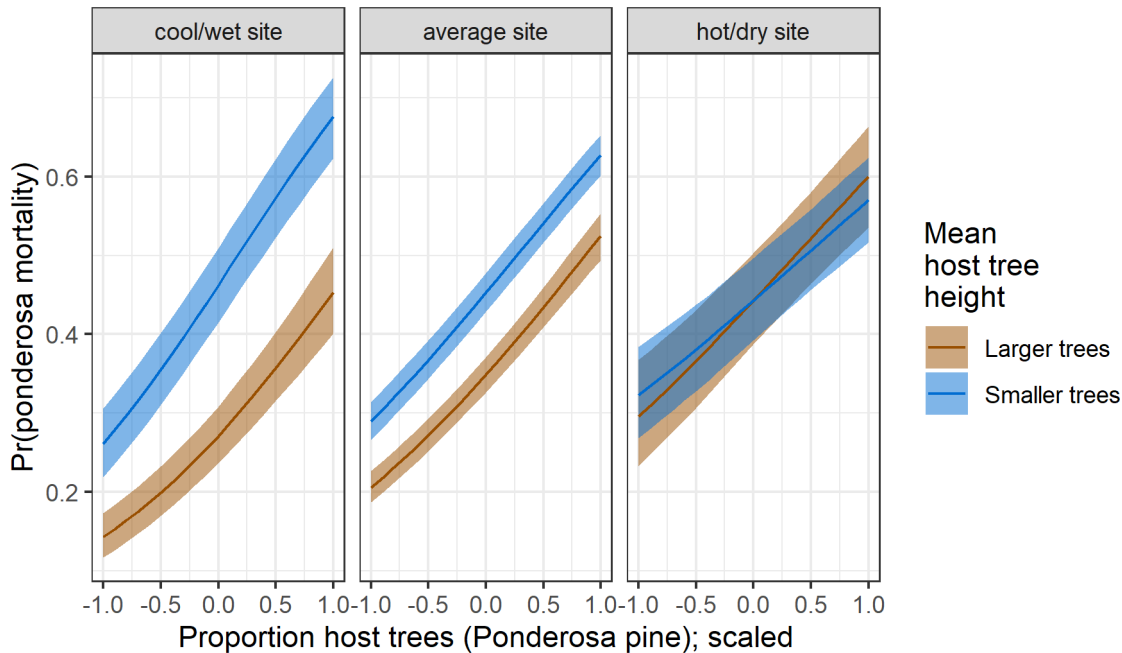


Figure 5: Line version of model results with 95% credible intervals showing primary influence of ponderosa pine structure on the probability of ponderosa pine mortality, and the interaction across climatic water deficit. The ‘larger trees’ line represents the mean height of ponderosa pine 0.7 standard deviations above the mean (approximately 24.1 m), and the ‘smaller trees’ line represents the mean height of ponderosa pine 0.7 standard deviations below the mean (approximately 12.1 m).

#### **442 Positive effect of host density and a negative effect of overall density**

443 A number of mechanisms associated with the relative abundance of species in a local area might underlie the  
 444 strong effect of host proportion on the probability of host tree mortality. Frequency-dependent herbivory—  
 445 whereby mixed-species forests experience less herbivory compared to monocultures (as an extreme example)—  
 446 is common, especially for oligophagous insect species (Jactel and Brockerhoff 2007). Furthermore, it has been  
 447 demonstrated that nonhost volatiles reduce attraction of several species of bark beetles to their aggregation  
 448 pheromones (Seybold et al. 2018), including WPB (Fettig et al. 2005). To that end, combinations of nonhost  
 449 volatiles and an antiaggregation pheromone have been used successfully to reduce levels of tree mortality  
 450 attributed to WPB (e.g., Fettig et al. 2012). In general, Hayes et al. (2009) and Fettig et al. (2019) found  
 451 that measures of host availability explained less variation in mortality than measures of overall tree density,  
 452 but those conclusions were based on a response variable of “total number of dead host trees,” rather than  
 453 the number of dead host trees conditional on the total number of host trees as in our study (i.e., a binomial  
 454 response).

455 The negative relationship between overall tree density and the probability of ponderosa pine mortality

456 corroborates findings of coincident ground plots (Fettig et al. 2019, in their analysis using proportion of  
457 trees killed as a response) and other work during the same hot drought (Restaino et al. 2019). The forest  
458 structure (in the absence of management) is itself a product of climate and, with increasing importance at  
459 finer spatial scales, topographic conditions (Fricker et al. 2019). Thus, the denser forest patches in our study  
460 may indicate greater local water availability, more favorable conditions for tree growth and survivorship,  
461 and increased resistance to beetle-induced mortality (Ma et al. 2010, Restaino et al. 2019, Fricker et al.  
462 2019). The negative two-way interaction between site CWD and overall density that amplifies the negative  
463 overall density effect in hotter, drier sites (effect size: -0.22; 95% CI: [-0.34, -0.11]) supports this explanation  
464 if greater local tree density implies especially favorable growing conditions (and locally resistant trees) when  
465 denser patches are found in hot, dry sites.

466 The positive relationship between host density and susceptibility to colonization by bark beetles has been so  
467 well-documented at the experimental plot level (e.g., Raffa and Berryman 1987, Oliver 1995) that lowering  
468 stand densities through selective harvest of hosts is commonly recommended for reducing future levels of tree  
469 mortality attributed to bark beetles (Fettig and Hilszczański 2015), including WPB (Fettig 2016). Greater  
470 host density shortens the flight distance required for WPB to disperse to new hosts, which likely facilitates  
471 bark beetle spread, however we calibrated our aerial tree detection to ~400 m<sup>2</sup> areas rather than to individual  
472 tree locations, so our data are insufficient to address these relationships. Increased density of ponderosa pine,  
473 specifically, may disproportionately increase the competitive environment for host trees (and thus increase  
474 their susceptibility to WPB colonization) if intraspecific competition amongst ponderosa pine trees is stronger  
475 than interspecific competition as would be predicted with coexistence theory (Chesson 2000). Finally, greater  
476 host densities increase the frequency that searching WPB land on hosts, rather than nonhosts, thus reducing  
477 the amount of energy expended during host finding and selection as well as the time that searching WPB  
478 spend exposed to predators.

#### 479 Positive interaction effect of CWD and basal area

480 While overall tree density is likely an indicator of favorable microsite in fire-suppressed forests, overall basal  
481 area is a better indicator of the local competitive environment especially in water-limited forests (Ma et al.  
482 2010, Fricker et al. 2019). While we found no main effect of overall basal area on the probability of ponderosa  
483 mortality, we did detect a clear interaction between site-level CWD and basal area such that mortality rates  
484 of ponderosa pine in hotter, drier sites were greater when local overall basal area was high.

485 **Negative main effect of host tree mean size, but strong positive interaction with site CWD**

486 The negative main effect of host tree mean size was surprising, and appears to contradict long-standing  
487 wisdom on the dynamics of western pine beetle in the Sierra Nevada. WPB exhibit a preference for trees 50.8  
488 to 76.2 cm in diameter at breast height (Person 1928, 1931), and a positive relationship between host tree  
489 size and levels of tree mortality attributed to WPB was reported by Fettig et al. (2019) in the coincident field  
490 plots as well as in other recent studies (Restaino et al. 2019, Stephenson et al. 2019, Pile et al. 2019). Indeed,  
491 Fettig et al. (2019) reported no mortality in ponderosa pine trees <10.0 cm DBH attributable to WPB and  
492 found no tree size/mortality relationship for incense cedar or white fir in the coincident field plots. This may  
493 reflect that bark beetles often attack the trees that are available even if they are suboptimal—especially those  
494 in the vicinity of larger, more desireable trees (Klein et al. 1978). At a broader scale, more small trees might  
495 be killed overall even though proportionally more larger trees are killed with respect to their frequency on  
496 the landscape (Klein et al. 1978).

497 These species represent 22.3% of the total tree mortality observed in their study, yet in our study all dead  
498 trees were classified as ponderosa pine (see Methods) which could dampen positive effect of tree size on  
499 mortality. Larger trees are more nutritious and are therefore ideal targets if local bark beetle density is high  
500 enough to successfully initiate mass attack as can occur when many trees are under severe water stress (Bentz  
501 et al. 2010, Kolb et al. 2016). In the recent hot drought, we expected that most trees would be under severe  
502 water stress, setting the stage for increasing beetle density, successful mass attacks, and targeting of larger  
503 trees. A possible explanation for our finding counter to this expectation is that our observations represent the  
504 cumulative mortality of trees during a multi-year drought event and its aftermath. Lower host tree mean size  
505 led to a greater probability of host mortality earlier in this drought (Pile et al. 2019, Stovall et al. 2019) and  
506 that signal might have persisted even as mortality continued to accumulate driven by other factors. Finally,  
507 tree growth rates may be a better predictor of susceptibility to WPB colonization than tree size per se, with  
508 slower-growing trees being most vulnerable (Miller and Keen 1960). While slow-growing trees are often also  
509 the largest trees, this may not be the case for our study sites especially given the legacy of fire exclusion  
510 in the Sierra Nevada and its effect of perturbing forest structure far outside its natural range of variation  
511 (Safford and Stevens 2017).

512 In hot, dry sites, larger average host size increased the probability of host mortality while smaller host sizes  
513 increased the probability of host mortality in cooler, wetter sites. Notably, a similar pattern was shown  
514 by Stovall et al. (2019) with a strong positive tree height/mortality relationship in areas with the greatest  
515 vapor pressure deficit and no tree height/mortality relationship in areas with the lowest vapor pressure

516 deficit. Stovall et al. (2019) did not observe that this environmental dependence extended to a negative tree  
517 height/mortality relationship (as we did) even at the lowest extremes of their vapor pressure deficit gradient,  
518 perhaps because their entire study took place in the southern Sierra Nevada which represents a hotter, drier  
519 portion of the more spatially extensive results we present here. Our work suggests that the WPB was cueing  
520 into different aspects of forest structure across an environmental gradient in a spatial context in a parallel  
521 manner to the temporal context noted by Stovall et al. (2019) and Pile et al. (2019), who observed that  
522 mortality was increasingly driven by larger trees as the hot drought proceeded and became more severe.

523 All of our sites were considered in an “epidemic” population phase for WPB (>5 trees killed per hectare; see  
524 Supplemental Information; Miller and Keen 1960, Hayes et al. 2009), but our results challenge the notion that  
525 outbreak behavior by the WPB and subsequent tree mortality is always driven by greater tree size. Despite a  
526 strong tree size/mortality relationship in coincident ground plots across our study area (Fettig et al. 2019),  
527 our results from surveying the broader context surrounding those ground plots reveals different effects of  
528 host tree size depending on CWD. Thus, it is possible that the massive tree mortality in hotter/drier Sierra  
529 Nevada forests (lower latitudes and elevations; Asner et al. 2016, Young et al. 2017) during the 2012 to  
530 2015 hot drought arose as a synergistic alignment of environmental conditions and local forest structure that  
531 allowed WPB to successfully colonize large trees, rapidly increase in population size, and expand. It follows  
532 that the unexpectedly low mortality in cooler/wetter Sierra Nevada forests compared to model predictions  
533 based on coarser-scale forest structure data (Young et al. 2017) could be explained by a different WPB  
534 response to local forest structure due to a lack of an alignment with favorable climate conditions.

## 535 Limitations and future directions

536 We have demonstrated that drones can be effective means of collecting forest data at multiple, vastly different  
537 spatial scales to investigate a single, multi-scale phenomenon— from meters in between trees, to hundreds  
538 of meters of elevation, to hundreds of thousands of meters of latitude. Some limitations remain but can be  
539 overcome with further refinements in the use of this tool for forest ecology. Most of these limitations arise  
540 from tree detection and classification uncertainty, and thus it was imperative to work with field data for  
541 calibration and uncertainty reporting.

542 The greatest limitation in our study arising from classification uncertainty is in the assumption that all dead  
543 trees were ponderosa pine, which we estimate from coincident field plots is true approximately 73.4% of  
544 the time. Because the forest structure factors influencing the likelihood of individual tree mortality during  
545 the hot drought depended on tree species (Stephenson et al. 2019), we cannot rule out that some of the

546 ponderosa pine mortality relationships to forest structure that we observed may be partially explained by  
547 those relationships in other species that were misclassified as ponderosa pine using our methods. However,  
548 the overall community composition across our study area was similar (Fettig et al. 2019) and we are able  
549 to reproduce similar forest structure/mortality patterns in drone-derived data when restricting the scope  
550 of analysis to only trees detected in the footprints of the coincident field plots with dramatically different  
551 patterns observed when including data from the forest surrounding the coincident field plots (see Supplemental  
552 information). Thus, we remain confident that the patterns we observed were driven primarily by the dynamic  
553 between WPB and ponderosa pine. While spectral information of foliage could help classify living trees to  
554 species, the species of standing dead trees were not spectrally distinct. This challenge of classifying standing  
555 dead trees to species implies that a conifer forest system with less bark beetle and tree host diversity, such  
556 as mountain pine beetle outbreaks in monocultures of lodgepole pine in the Intermountain West, should be  
557 particularly amenable to the methods presented here even with minimal further refinement because dead  
558 trees will almost certainly belong to a single species and have succumbed to colonization by a single bark  
559 beetle species.

560 Some uncertainty surrounded our ability to detect trees using the geometry of the dense point clouds derived  
561 with SfM. The horizontal accuracy of the tree detection was better than the vertical accuracy, which may  
562 result from a more significant error contribution by the field-based calculations of tree height compared to  
563 tree position relative to plot center (Table 2). Both the horizontal and vertical accuracy would likely improve  
564 with better SfM point clouds, which can be enhanced with greater overlap between images (Frey et al. 2018)  
565 or with oblique (i.e., off-nadir) imagery (James and Robson 2014). Frey et al. (2018) found that 95% overlap  
566 was preferable for generating dense point clouds in forested areas, and James and Robson (2014) reduced  
567 dense point cloud errors using imagery taken at 30 degrees off-nadir. We only achieved 91.6% overlap with  
568 the X3 RGB camera and 83.9% overlap with the multispectral camera, and all imagery was nadir-facing.  
569 While our live/dead classification was fairly accurate (96.4% on a withheld dataset), our species classifier  
570 would likely benefit from better crown segmentation because the pixel-level reflectance values within each  
571 crown are averaged to characterize the “spectral signature” of each tree. With better delineation of each  
572 tree crown, the mean value of pixels within each tree crown will likely be more representative of that tree’s  
573 spectral signature. Better crown segmentation might most readily be achieved through greater overlap in  
574 imagery. Finally, we anticipate that computer vision and deep learning will prove helpful in overcoming some  
575 of these detection and classification challenges (Gray et al. 2019).

<sup>576</sup> **Conclusions**

<sup>577</sup> Climate change adaptation strategies emphasize management action that considers whole-ecosystem responses  
<sup>578</sup> to inevitable change (Millar et al. 2007), which requires a macroecological understanding of how phenomena at  
<sup>579</sup> multiple scales can interact. Tree vulnerability to environmental stressors presents only a partial explanation  
<sup>580</sup> for tree mortality patterns during hot droughts, especially when bark beetles are present. We've shown that  
<sup>581</sup> drones can be a valuable tool for investigating multi-scalar phenomena, such as how local forest structure  
<sup>582</sup> combines with environmental conditions to shape forest insect disturbance. Understanding the conditions  
<sup>583</sup> that drive dry western U.S. forest responses to disturbances such as bark beetle outbreaks will be vital for  
<sup>584</sup> predicting outcomes from increasing disturbance frequency and intensity exacerbated by climate change. Our  
<sup>585</sup> study suggests that outcomes will depend on interactions between local forest structure and broad-scale  
<sup>586</sup> environmental gradients, with the potential for cross-scale interactions to enhance our current understanding  
<sup>587</sup> of forest insect dynamics.

588 **References**

- 589 Anderegg, W. R. L., J. A. Hicke, R. A. Fisher, C. D. Allen, J. Aukema, B. Bentz, S. Hood, J. W. Lichstein,  
590 A. K. Macalady, N. McDowell, Y. Pan, K. Raffa, A. Sala, J. D. Shaw, N. L. Stephenson, C. Tague, and  
591 M. Zeppel. 2015. Tree mortality from drought, insects, and their interactions in a changing climate. *New*  
592 *Phytologist* 208:674–683.
- 593 Asner, G. P., P. G. Brodrick, C. B. Anderson, N. Vaughn, D. E. Knapp, and R. E. Martin. 2016. Progressive  
594 forest canopy water loss during the 2012–2015 California drought. *Proceedings of the National Academy of*  
595 *Sciences* 113:E249–E255.
- 596 Baldwin, B. G., A. H. Thornhill, W. A. Freyman, D. D. Ackerly, M. M. Kling, N. Morueta-Holme, and B. D.  
597 Mishler. 2017. Species richness and endemism in the native flora of California. *American Journal of Botany*  
598 104:487–501.
- 599 Bedard, W. D., P. E. Tilden, D. L. Wood, R. M. Silverstein, R. G. Brownlee, and J. O. Rodin. 1969.  
600 Western pine beetle: Field response to its sex pheromone and a synergistic host terpene, myrcene. *Science*  
601 164:1284–1285.
- 602 Bentz, B. J., J. Régnière, C. J. Fettig, E. M. Hansen, J. L. Hayes, J. A. Hicke, R. G. Kelsey, J. F. Negrón,  
603 and S. J. Seybold. 2010. Climate change and bark beetles of the western United States and Canada: Direct  
604 and indirect effects. *BioScience* 60:602–613.
- 605 Berryman, A. A. 1982. Population dynamics of bark beetles. Pages 264–314 in *Bark Beetles in North*  
606 *American Conifers: A System for the Study of Evolutionary Biology*.
- 607 Boone, C. K., B. H. Aukema, J. Bohlmann, A. L. Carroll, and K. F. Raffa. 2011. Efficacy of tree defense  
608 physiology varies with bark beetle population density: A basis for positive feedback in eruptive species.  
609 *Canadian Journal of Forest Research* 41:1174–1188.
- 610 Brooks, S. P., and A. Gelman. 1998. General methods for monitoring convergence of iterative simulations.  
611 *Journal of Computational and Graphical Statistics* 7:434.
- 612 Bürkner, P.-C. 2017. **brms**: An *R* package for bayesian multilevel models using *Stan*. *Journal of Statistical*  
613 *Software* 80:1–28.
- 614 Byers, J. A., and D. L. Wood. 1980. Interspecific inhibition of the response of the bark beetles, *Dendroctonus*  
615 *brevicomis* and *Ips paraconfusus*, to their pheromones in the field. *Journal of Chemical Ecology* 6:149–164.
- 616 Carpenter, B., A. Gelman, M. D. Hoffman, D. Lee, B. Goodrich, M. Betancourt, M. Brubaker, J. Guo, P. Li,

- 617 and A. Riddell. 2017. Stan: A Probabilistic Programming Language. *Journal of Statistical Software* 76:1–32.
- 618 Chesson, P. 2000. Mechanisms of maintenance of species diversity. *Annual Review of Ecology and Systematics*  
619 31:343–366.
- 620 Chubaty, A. M., B. D. Roitberg, and C. Li. 2009. A dynamic host selection model for mountain pine beetle,  
621 *Dendroctonus ponderosae* Hopkins. *Ecological Modelling* 220:1241–1250.
- 622 Clevers, J., and A. Gitelson. 2013. Remote estimation of crop and grass chlorophyll and nitrogen content using  
623 red-edge bands on Sentinel-2 and -3. *International Journal of Applied Earth Observation and Geoinformation*  
624 23:344–351.
- 625 Coops, N. C., M. Johnson, M. A. Wulder, and J. C. White. 2006. Assessment of QuickBird high spatial  
626 resolution imagery to detect red attack damage due to mountain pine beetle infestation. *Remote Sensing of*  
627 *Environment* 103:67–80.
- 628 DJI. 2015a. Zenmuse X3 - Creativity Unleashed. <https://www.dji.com/zenmuse-x3/info>.
- 629 DJI. 2015b. DJI - The World Leader in Camera Drones/Quadcopters for Aerial Photography. <https://www.dji.com/matrice100/info>.
- 631 DronesMadeEasy. 2018. Map Pilot for DJI on iOS. [https://itunes.apple.com/us/app/map-pilot-for-dji/  
632 id1014765000?mt=8](https://itunes.apple.com/us/app/map-pilot-for-dji/id1014765000?mt=8).
- 633 Evenden, M. L., C. M. Whitehouse, and J. Sykes. 2014. Factors influencing flight capacity of the mountain  
634 pine beetle (Coleoptera: Curculionidae: Scolytinae). *Environmental Entomology* 43:187–196.
- 635 Eysn, L., M. Hollaus, E. Lindberg, F. Berger, J.-M. Monnet, M. Dalponte, M. Kobal, M. Pellegrini, E.  
636 Lingua, D. Mongus, and N. Pfeifer. 2015. A benchmark of LiDAR-based single tree detection methods using  
637 heterogeneous forest data from the alpine space. *Forests* 6:1721–1747.
- 638 Farr, T. G., P. A. Rosen, E. Caro, R. Crippen, R. Duren, S. Hensley, M. Kobrick, M. Paller, E. Rodriguez, L.  
639 Roth, D. Seal, S. Shaffer, J. Shimada, J. Umland, M. Werner, M. Oskin, D. Burbank, and D. Alsdorf. 2007.  
640 The shuttle radar topography mission. *Reviews of Geophysics* 45.
- 641 Fettig, C. J. 2012. Chapter 2: Forest health and bark beetles. *in* Managing Sierra Nevada Forests. PSW-  
642 GTR-237. USDA Forest Service.
- 643 Fettig, C. J. 2016. Native bark beetles and wood borers in Mediterranean forests of California. Pages 499–528  
644 *in* Insects and diseases of Mediterranean Forest systems. Springer International Publishing, Switzerland.

- 645 Fettig, C. J., and J. Hilszczański. 2015. Management strategies for bark beetles in conifer forests. Pages  
646 555–584 in Bark Beetles. Elsevier.
- 647 Fettig, C. J., K. D. Klepzig, R. F. Billings, A. S. Munson, T. E. Nebeker, J. F. Negrón, and J. T. Nowak. 2007.  
648 The effectiveness of vegetation management practices for prevention and control of bark beetle infestations in  
649 coniferous forests of the western and southern United States. Forest Ecology and Management 238:24–53.
- 650 Fettig, C. J., S. R. McKelvey, C. P. Dabney, D. P. W. Huber, C. G. Lait, D. L. Fowler, and J. H. Borden. 2012.  
651 Efficacy of “Verbenone Plus” for protecting ponderosa pine trees and stands from *Dendroctonus brevicomis*  
652 (Coleoptera: Curculionidae) attack in British Columbia and California. Journal of Economic Entomology  
653 105:1668–1680.
- 654 Fettig, C. J., S. R. McKelvey, and D. P. W. Huber. 2005. Nonhost angiosperm volatiles and Verbenone disrupt  
655 response of western pine beetle, *Dendroctonus brevicomis* (Coleoptera: Scolytidae), to attractant-baited traps.  
656 Journal of Economic Entomology 98:2041–2048.
- 657 Fettig, C. J., L. A. Mortenson, B. M. Bulaon, and P. B. Foulk. 2019. Tree mortality following drought in the  
658 central and southern Sierra Nevada, California, U.S. Forest Ecology and Management 432:164–178.
- 659 Flint, L. E., A. L. Flint, J. H. Thorne, and R. Boynton. 2013. Fine-scale hydrologic modeling for regional land-  
660 scape applications: The California Basin Characterization Model development and performance. Ecological  
661 Processes 2:25.
- 662 Floyd, M. L., M. Clifford, N. S. Cobb, D. Hanna, R. Delph, P. Ford, and D. Turner. 2009. Relationship of  
663 stand characteristics to drought-induced mortality in three Southwestern piñonJuniper woodlands. Ecological  
664 Applications 19:1223–1230.
- 665 Franceschi, V. R., P. Krokene, E. Christiansen, and T. Krekling. 2005. Anatomical and chemical defenses of  
666 conifer bark against bark beetles and other pests. New Phytologist 167:353–376.
- 667 Frey, J., K. Kovach, S. Stemmler, and B. Koch. 2018. UAV photogrammetry of forests as a vulnerable  
668 process. A sensitivity analysis for a structure from motion RGB-image pipeline. Remote Sensing 10:912.
- 669 Fricker, G. A., N. W. Synes, J. M. Serra-Diaz, M. P. North, F. W. Davis, and J. Franklin. 2019. More than  
670 climate? Predictors of tree canopy height vary with scale in complex terrain, Sierra Nevada, CA (USA).  
671 Forest Ecology and Management 434:142–153.
- 672 Gabry, J., D. Simpson, A. Vehtari, M. Betancourt, and A. Gelman. 2019. Visualization in Bayesian workflow.  
673 Journal of the Royal Statistical Society: Series A (Statistics in Society) 182:389–402.

- 674 Geiszler, D. R., and R. I. Gara. 1978. Mountain pine beetle attack dynamics in lodgepole pine. *in* Theory  
675 and Practice of Mountain Pine Beetle Management in Lodgepole Pine Forests: Symposium Proceedings. A.  
676 A. Berryman, G. D. Amman and R. W. Stark (Eds). Pullman, WA, USA.
- 677 Gitelson, A., and M. N. Merzlyak. 1994. Spectral reflectance changes associated with autumn senescence of  
678 *Aesculus hippocastanum* L. And *Acer platanoides* L. Leaves. Spectral features and relation to chlorophyll  
679 estimation. *Journal of Plant Physiology* 143:286–292.
- 680 Graf, M., M. Reid, B. Aukema, and B. Lindgren. 2012. Association of tree diameter with body size and lipid  
681 content of mountain pine beetles. *The Canadian Entomologist* 144:467–477.
- 682 Gray, P. C., A. B. Fleishman, D. J. Klein, M. W. McKown, V. S. Bézy, K. J. Lohmann, and D. W. Johnston.  
683 2019. A convolutional neural network for detecting sea turtles in drone imagery. *Methods in Ecology and  
684 Evolution* 10:345–355.
- 685 Griffin, D., and K. J. Anchukaitis. 2014. How unusual is the 2012-2014 California drought? *Geophysical  
686 Research Letters* 41:9017–9023.
- 687 Hayes, C. J., C. J. Fettig, and L. D. Merrill. 2009. Evaluation of multiple funnel traps and stand characteristics  
688 for estimating western pine beetle-caused tree mortality. *Journal of Economic Entomology* 102:2170–2182.
- 689 Hijmans, R. J., J. van Etten, M. Sumner, J. Cheng, A. Bevan, R. Bivand, L. Busetto, M. Canty, D. Forrest,  
690 A. Ghosh, D. Golicher, J. Gray, J. A. Greenberg, P. Hiemstra, I. for M. A. Geosciences, C. Karney, M.  
691 Mattiuzzi, S. Mosher, J. Nowosad, E. Pebesma, O. P. Lamigueiro, E. B. Racine, B. Rowlingson, A. Shortridge,  
692 B. Venables, and R. Wueest. 2019. Raster: Geographic data analysis and modeling.
- 693 Hoffman, M. D., and A. Gelman. 2014. The No-U-Turn Sampler: Adaptively setting path lengths in  
694 Hamiltonian Monte Carlo. *Journal of Machine Learning Research* 15:31.
- 695 Hunziker, P. 2017. Velox: Fast raster manipulation and extraction.
- 696 Jactel, H., and E. G. Brockerhoff. 2007. Tree diversity reduces herbivory by forest insects. *Ecology Letters*  
697 10:835–848.
- 698 Jakubowski, M. K., W. Li, Q. Guo, and M. Kelly. 2013. Delineating individual trees from LiDAR data: A  
699 comparison of vector- and raster-based segmentation approaches. *Remote Sensing* 5:4163–4186.
- 700 James, M. R., and S. Robson. 2014. Mitigating systematic error in topographic models derived from UAV  
701 and ground-based image networks. *Earth Surface Processes and Landforms* 39:1413–1420.
- 702 Jeronimo, S. M. A., V. R. Kane, D. J. Churchill, J. A. Lutz, M. P. North, G. P. Asner, and J. F. Franklin.

- 703 2019. Forest structure and pattern vary by climate and landform across active-fire landscapes in the montane  
704 Sierra Nevada. *Forest Ecology and Management* 437:70–86.
- 705 Kaiser, K. E., B. L. McGlynn, and R. E. Emanuel. 2013. Ecohydrology of an outbreak: Mountain pine beetle  
706 impacts trees in drier landscape positions first: ECOHYDROLOGY OF A MOUNTAIN PINE BEETLE  
707 OUTBREAK. *Ecohydrology* 6:444–454.
- 708 Kane, V. R., M. P. North, J. A. Lutz, D. J. Churchill, S. L. Roberts, D. F. Smith, R. J. McGaughey, J. T.  
709 Kane, and M. L. Brooks. 2014. Assessing fire effects on forest spatial structure using a fusion of Landsat and  
710 airborne LiDAR data in Yosemite National Park. *Remote Sensing of Environment* 151:89–101.
- 711 Klein, W. H., D. L. Parker, and C. E. Jensen. 1978. Attack, emergence, and stand depletion trends of the  
712 mountain pine beetle in a lodgepole pine stand during an outbreak. *Environmental Entomology* 7:732–737.
- 713 Kolb, T. E., C. J. Fettig, M. P. Ayres, B. J. Bentz, J. A. Hicke, R. Mathiasen, J. E. Stewart, and A. S. Weed.  
714 2016. Observed and anticipated impacts of drought on forest insects and diseases in the United States. *Forest  
715 Ecology and Management* 380:321–334.
- 716 Kuhn, M. 2008. Building predictive models in R using the caret package. *Journal of Statistical Software*  
717 28:1–26.
- 718 Larson, A. J., and D. Churchill. 2012. Tree spatial patterns in fire-frequent forests of western North America,  
719 including mechanisms of pattern formation and implications for designing fuel reduction and restoration  
720 treatments. *Forest Ecology and Management* 267:74–92.
- 721 Li, W., Q. Guo, M. K. Jakubowski, and M. Kelly. 2012. A new method for segmenting individual trees from  
722 the LiDAR point cloud. *Photogrammetric Engineering & Remote Sensing* 78:75–84.
- 723 Logan, J. A., P. White, B. J. Bentz, and J. A. Powell. 1998. Model analysis of spatial patterns in mountain  
724 pine beetle outbreaks. *Theoretical Population Biology* 53:236–255.
- 725 Ma, S., A. Concilio, B. Oakley, M. North, and J. Chen. 2010. Spatial variability in microclimate in a  
726 mixed-conifer forest before and after thinning and burning treatments. *Forest Ecology and Management*.  
727 259: 904–915 259:904–915.
- 728 Meyer, F., and S. Beucher. 1990. Morphological segmentation. *Journal of Visual Communication and Image  
729 Representation* 1:21–46.
- 730 Micasense. 2015. MicaSense. <https://support.micasense.com/hc/en-us/articles/215261448-RedEdge-User-Manual-PDF-Download->.

- 732 Millar, C. I., N. L. Stephenson, and S. L. Stephens. 2007. Climate change and forests of the future: Managing  
733 in the face of uncertainty. *Ecological Applications* 17:2145–2151.
- 734 Millar, C. I., R. D. Westfall, D. L. Delany, M. J. Bokach, A. L. Flint, and L. E. Flint. 2012. Forest mortality in  
735 high-elevation whitebark pine (*Pinus albicaulis*) forests of eastern California, USA: Influence of environmental  
736 context, bark beetles, climatic water deficit, and warming. *Canadian Journal of Forest Research* 42:749–765.
- 737 Miller, J. M., and F. P. Keen. 1960. Biology and control of the western pine beetle: A summary of the first  
738 fifty years of research. US Department of Agriculture.
- 739 Mitchell, R. G., and H. K. Preisler. 1991. Analysis of spatial patterns of lodgepole pine attacked by outbreak  
740 populations of the mountain pine beetle. *Forest Science* 37:1390–1408.
- 741 Moeck, H. A., D. L. Wood, and K. Q. Lindahl. 1981. Host selection behavior of bark beetles (Coleoptera:  
742 Scolytidae) attacking *Pinus ponderosa*, with special emphasis on the western pine beetle, *Dendroctonus*  
743 *brevicomis*. *Journal of Chemical Ecology* 7:49–83.
- 744 Morris, J. L., S. Cottrell, C. J. Fettig, W. D. Hansen, R. L. Sherriff, V. A. Carter, J. L. Clear, J. Clement, R.  
745 J. DeRose, J. A. Hicke, P. E. Higuera, K. M. Mattor, A. W. R. Seddon, H. T. Seppä, J. D. Stednick, and S.  
746 J. Seybold. 2017. Managing bark beetle impacts on ecosystems and society: Priority questions to motivate  
747 future research. *Journal of Applied Ecology* 54:750–760.
- 748 Oliver, W. W. 1995. Is self-thinning in ponderosa pine ruled by *Dendroctonus* bark beetles? Page 6 in Forest  
749 health through silviculture: Proceedings of the 1995 National Silviculture Workshop.
- 750 Pau, G., F. Fuchs, O. Sklyar, M. Boutros, and W. Huber. 2010. EBImage: An R package for image processing  
751 with applications to cellular phenotypes. *Bioinformatics* 26:979–981.
- 752 Person, H. L. 1928. Tree selection by the western pine beetle. *Journal of Forestry* 26:564–578.
- 753 Person, H. L. 1931. Theory in explanation of the selection of certain trees by the western pine beetle. *Journal*  
754 *of Forestry* 29:696–699.
- 755 Pile, L. S., M. D. Meyer, R. Rojas, O. Roe, and M. T. Smith. 2019. Drought impacts and compounding  
756 mortality on forest trees in the southern Sierra Nevada. *Forests* 10:237.
- 757 Plowright, A. 2018. ForestTools: Analyzing remotely sensed forest data.
- 758 Preisler, H. K. 1993. Modelling Spatial Patterns of Trees Attacked by Bark-Beetles. *Applied Statistics* 42:501.
- 759 R Core Team. 2018. R: A language and environment for statistical computing. R Foundation for Statistical  
760 Computing, Vienna, Austria.

- 761 Raffa, K. F., B. H. Aukema, B. J. Bentz, A. L. Carroll, J. A. Hicke, M. G. Turner, and W. H. Romme. 2008.
- 762 Cross-scale drivers of natural disturbances prone to anthropogenic amplification: The dynamics of bark beetle
- 763 eruptions. *BioScience* 58:501–517.
- 764 Raffa, K. F., and A. A. Berryman. 1983. The role of host plant resistance in the colonization behavior and
- 765 ecology of bark beetles (Coleoptera: Scolytidae). *Ecological Monographs* 53:27–49.
- 766 Raffa, K. F., and A. A. Berryman. 1987. Interacting selective pressures in conifer-bark beetle systems: A
- 767 basis for reciprocal adaptations? *The American Naturalist* 129:234–262.
- 768 Raffa, K. F., J.-C. Grégoire, and B. Staffan Lindgren. 2015. Natural history and ecology of bark beetles.
- 769 Pages 1–40 in *Bark Beetles*. Elsevier.
- 770 Restaino, C., D. Young, B. Estes, S. Gross, A. Wuenschel, M. Meyer, and H. Safford. 2019. Forest
- 771 structure and climate mediate drought-induced tree mortality in forests of the Sierra Nevada, USA. *Ecological*
- 772 *Applications* 0:e01902.
- 773 Robeson, S. M. 2015. Revisiting the recent California drought as an extreme value. *Geophysical Research*
- 774 *Letters* 42:6771–6779.
- 775 Rouse, W., R. H. Haas, W. Deering, and J. A. Schell. 1973. Monitoring the vernal advancement and
- 776 retrogradation (green wave effect) of natural vegetation. Type II Report, Goddard Space Flight Center,
- 777 Greenbelt, MD, USA.
- 778 Roussel, J.-R. 2019. lidRplugins: Extra functions and algorithms for lidR package.
- 779 Roussel, J.-R., D. Auty, F. De Boissieu, and A. S. Meador. 2019. lidR: Airborne LiDAR data manipulation
- 780 and visualization for forestry applications.
- 781 Safford, H. D., and J. T. Stevens. 2017. Natural range of variation for yellow pine and mixed-conifer forests
- 782 in the Sierra Nevada, Southern Cascades, and Modoc and Inyo National Forests, California, USA. Page 241.
- 783 dos Santos, A. A., J. Marcato Junior, M. S. Araújo, D. R. Di Martini, E. C. Tetila, H. L. Siqueira, C. Aoki, A.
- 784 Eltner, E. T. Matsubara, H. Pistori, R. Q. Feitosa, V. Liesenberg, and W. N. Gonçalves. 2019. Assessment of
- 785 CNN-Based Methods for Individual Tree Detection on Images Captured by RGB Cameras Attached to UAVs.
- 786 Sensors (Basel, Switzerland) 19.
- 787 Seidl, R., J. Müller, T. Hothorn, C. Bässler, M. Heurich, and M. Kautz. 2016. Small beetle, large-scale
- 788 drivers: How regional and landscape factors affect outbreaks of the European spruce bark beetle. *The Journal*
- 789 *of applied ecology* 53:530–540.

- 790 Senf, C., E. M. Campbell, D. Pflugmacher, M. A. Wulder, and P. Hostert. 2017. A multi-scale analysis of  
791 western spruce budworm outbreak dynamics. *Landscape Ecology* 32:501–514.
- 792 Seybold, S. J., B. J. Bentz, C. J. Fettig, J. E. Lundquist, R. A. Progar, and N. E. Gillette. 2018. Management  
793 of western North American bark beetles with semiochemicals. *Annual Review of Entomology* 63:407–432.
- 794 Shepherd, W. P., D. P. W. Huber, S. J. Seybold, and C. J. Fettig. 2007. Antennal responses of the western  
795 pine beetle, *Dendroctonus brevicomis* (Coleoptera: Curculionidae), to stem volatiles of its primary host,  
796 *Pinus ponderosa*, and nine sympatric nonhost angiosperms and conifers. *Chemoecology* 17:209–221.
- 797 Shiklomanov, A. N., B. A. Bradley, K. M. Dahlin, A. M. Fox, C. M. Gough, F. M. Hoffman, E. M. Middleton,  
798 S. P. Serbin, L. Smallman, and W. K. Smith. 2019. Enhancing global change experiments through integration  
799 of remote-sensing techniques. *Frontiers in Ecology and the Environment* 0.
- 800 Shin, P., T. Sankey, M. Moore, and A. Thode. 2018. Evaluating unmanned aerial vehicle images for estimating  
801 forest canopy fuels in a ponderosa pine stand. *Remote Sensing* 10:1266.
- 802 Stephenson, N. 1998. Actual evapotranspiration and deficit: Biologically meaningful correlates of vegetation  
803 distribution across spatial scales. *Journal of Biogeography* 25:855–870.
- 804 Stephenson, N. L., A. J. Das, N. J. Ampersee, and B. M. Bulaon. 2019. Which trees die during drought?  
805 The key role of insect host-tree selection. *Journal of Ecology*:75.
- 806 Stovall, A. E. L., H. Shugart, and X. Yang. 2019. Tree height explains mortality risk during an intense  
807 drought. *Nature Communications* 10:1–6.
- 808 Thistle, H. W., H. Peterson, G. Allwine, B. Lamb, T. Strand, E. H. Holsten, and P. J. Shea. 2004. Surrogate  
809 pheromone plumes in three forest trunk spaces: Composite statistics and case studies. *Forest Science* 50.
- 810 USDAFS. 2019, February 11. Press Release: Survey finds 18 million trees died in California in 2018.  
811 [https://www.fs.usda.gov/Internet/FSE\\_DOCUMENTS/FSEPRD609321.pdf](https://www.fs.usda.gov/Internet/FSE_DOCUMENTS/FSEPRD609321.pdf).
- 812 Vega, C., A. Hamrouni, S. El Mokhtari, J. Morel, J. Bock, J. P. Renaud, M. Bouvier, and S. Durrieu. 2014.  
813 PTrees: A point-based approach to forest tree extraction from LiDAR data. *International Journal of Applied  
814 Earth Observation and Geoinformation* 33:98–108.
- 815 Wallin, K. F., and K. F. Raffa. 2004. Feedback between Individual Host Selection Behavior and Population  
816 Dynamics in an Eruptive Herbivore. *Ecological Monographs* 74:101–116.
- 817 Weinstein, B. G., S. Marconi, S. Bohlman, A. Zare, and E. White. 2019. Individual Tree-Crown Detection in  
818 RGB Imagery Using Semi-Supervised Deep Learning Neural Networks. *Remote Sensing* 11:1309.

- 819 Wyngaard, J., L. Barbieri, A. Thomer, J. Adams, D. Sullivan, C. Crosby, C. Parr, J. Klump, S. Raj Shrestha,  
820 and T. Bell. 2019. Emergent challenges for science sUAS data management: Fairness through community  
821 engagement and best practices development. *Remote Sensing* 11:1797.
- 822 Young, D. J. N., J. T. Stevens, J. M. Earles, J. Moore, A. Ellis, A. L. Jirka, and A. M. Latimer. 2017.  
823 Long-term climate and competition explain forest mortality patterns under extreme drought. *Ecology Letters*  
824 20:78–86.
- 825 Zhang, W., J. Qi, P. Wan, H. Wang, D. Xie, X. Wang, and G. Yan. 2016. An easy-to-use airborne LiDAR  
826 data filtering method based on cloth simulation. *Remote Sensing* 8:501.